Mechanically Produced Sub-Micro and Nano Powders of Mg and Mg/Carbon Composites as Anode Material of Primary and Secondary Mg-Air Batteries

Hassan Karami[*], **Foroozandeh Taala, Reza Behjat-Manesh Ardakani, Mohammad Ali Karimi**

Department of Chemistry, Payame Noor University Box 19395-4697, Tehran, Iran

Abstract

In this work, sub-micro and nanometer sized Mg and Mg/carbon composites as anode materials of Mg-air batteries is prepared by using an innovative rotary ball mill. Characterization of the prepared samples is performed by dynamic light scattering, scanning electron microscopy, transmission electron microscopy and, X-ray diffraction techniques. The effects of milling time and amount of carbon additive are evaluated on the sizes of Mg particles in different samples, the discharge capacities and also other electrochemical performances of both primary and secondary magnesium air batteries. An aqueous solution of 2 M Magnesium Chloride and 3 M Sodium Chloride and an organic solution of 0.2 M I_2 in Dimethyl Sulfoxide are used as electrolytes in primary and secondary Mg-air batteries, respectively. The Mg sample T_6 with average particle size of 170 nm and the Mg/carbon composite sample T_{13} with average particle size of 35 nm show the highest discharge capacities in both primary (333.1 and 418.6 mA.h g^{-1}) and secondary (354.4 and 433.9 mA.h g^{-1}) Mg-air batteries, respectively. The cycle life test was examined on all constructed rechargeable Mg-air batteries over 30 cycles.

1. INTRODUCTION

In today's world, the supply of energy through the over-consumption of fossil fuels has caused to enter pollutants into water, soil and air. Therefore, finding new ways to generate new and clean energy without greenhouse gases is necessary. The batteries are the most important and most widely useful sources of electrical energy are which are widely used in different applications [1]. Between different batteries, metal-air batteries has shown a ray of hope in the research path to develop low cost and low volume metal-air batteries with high energy density, long life and without greenhouse gas emissions [2-7]. Lightweight of metal-air batteries is due to the air oxygen as the cathode substance [8]. Corrosion of anode in electrolyte and dependency of battery performance on environmental conditions such as temperature case limitation in development of metal-air batteries [1]. The primary magnesium-air batteries (PMABs) or Mg-air fuel cells has attracted much attention. For more than 50 years, magnesium fuel cells have been manufactured and used by some companies [4]. Magnesium as anode of metal-air batteries has some advantages such as reasonable prices, abundance in the world, environmental compatibility, proper safety, low toxicity and high potential (-2.37 V vs. SHE) [3-8]. The anode and cathode reactions in PMABs were done according to Equations 1 to 3 [8]:

Anode: $2Mg + 4OH^- \rightarrow 2Mg(OH)_2 + 4e^-$ E_0
                 $= -2.69\,V$ (1)

Cathode: $O_2 + 2H_2O + 4e^- \rightarrow 4OH^-$ E_0
                 $= 0.4\,V$ (2)

Overall: $2Mg + O_2 + 2H_2O$
              $\rightarrow 2Mg(OH)_2$ $E_{overall}$
              $= 3.09\,V$ (3)
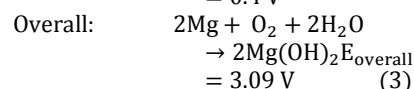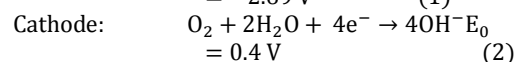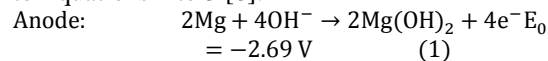
According to the above mentioned reactions, the appropriate choice of electrolyte, anode and cathode materials are of great importance [4,8]. Mg/O_2 batteries due to the high theoretical voltage (-3.09 V), high specific capacity (2205 mA.h g^{-1}) and, big energy density (3910 Wh Kg^{-1}), low toxicity and abundant reserves in both the earthʾs crust and sea water is one of the most attractive and most suitable anode material in metal-air batteries [6-8]. Due to the high self-discharge, slow kinetics and insoluble discharge products ($Mg(OH)_2$, MgO and MgO_2), the coulombic efficiency, shelf life and electrochemical performance of Mg-air batteries are smaller than those of theoretical values [9,10]. The PMABs have a special place as energy sources because of can be easily assembled and metal anodes can be mechanically charged [11,12], so

* Corresponding author:
H. Karami; E-mail: Karami.hassan@pnu.ac.ir , karami_h@yahoo.com

that these are designed as a rechargeable battery, in contrast the actual rechargeable type with reversible reactions is prepared with nonaqueous electrolyte [13,14].

In secondary magnesium-air batteries (SMABs), there are three challenges: (1) finding Mg-based materials that be fully charged, (2) finding suitable electrolytes without any reaction with discharged products and (3) finding highly active electrocatalyst that both react to oxygen reduction and release, which reduces the polarization and accelerates the decomposition of discharge products on surface anode electrode [15-17].

The choice of anodic material for SMABs is critical factor. Using of mesoporous and nanostructured Mg as anode materials is the one suggestion to improve battery performance [18-20]. Applying magnesium micro/meso/nano structures are also a reasonable strategy to reduce the kinetics of inactive film formation on the surface of anode [21]. Increasing the specific surface area in sub micro and nano structures of Mg material, decreases the actual density of the electrode during the discharge process, thereby polarization of the Mg electrode reducing, which improves the energy density and discharge rate of the battery. There are many scientific reports about the improvement if Mg/O_2 batteries using different micro/meso/nano structures of Mg [18,22-26].

Alloying of Mg with other elements is common ways to improve the properties of magnesium as an active anode so that increases battery performance. Many elements as impurity in Mg anode such as iron, cobalt or nickel reduce the battery performance [2,10,15,27-30]. Based on the scientific research, the purity of initial Mg material and the element type for alloying with Mg is most important.

The performance of metal-air battery is highly depends on the structure of cathode. On the cathode electrode, the O_2 molecules are catalytically reduced. The structure of an oxygen cathode consists of at least three layers: (1) a waterproof breathable layer for the separation of electrolyte and gas (for example Teflon), (2) a carbon porous layer for oxygen gas penetration and electrical conductivity, and (3) a catalyst layer made of noble metals such as Pt, Ag, Pd, Au.

Choice of suitable electrolyte as well as anode and cathode is vital to improve the electrochemical performance of $Mg-O_2$ batteries . A suitable electrolyte should be able to made uniform corrosion of the magnesium anode at a minimum rate, minimal polarization and the rapid deposition of the anodic product ($Mg(OH)_2$) on the anode electrode [11]. For example, Shihirova et al. suggested sodium nitrate and sodium salicylate as electrolyte additive in mag-air batteries to improve discharge rate [31] or, Park et al. studied the effect of electrolyte circulation on the performance of magnesium-air batteries (MABs) [32]. There are many reports about nonaqueous, ionic liquids and hybrid electrolytes as a suitable choice to achieve rechargeability in MABs. Shiga et al. studied iodine–dimethyl sulfoxide (I_2–DMSO) complex as an electrolyte in SMABs. They proved that the presence of I_2 in Dimethyl sulfoxide (DMSO) improves the rechargeability of MABs [33]. According to Ref. 33, I2 interact with DMSO to form I_2-DMSO complex which can release I_2 molecules during discharge. During the discharge, Mg^{2+} ions interact with oxygen species in aprotic solvents to form MgO at the cathode surface. MgO is a thermodynamically and electrochemically stable material. Therefore, the produced MgO on the cathode surface cannot be reduced to Mg by charging at ambient temperatures. Without catalytic agent, it is expected that organic Mg– air batteries as well as aqueous Mg-air batteries operate as primary cells. Shiga et al. described that the I_2 molecules can react with MgO to reform Mg^{2+} ions as MgI_2 ($MgO+I_2 \rightarrow MgI_2 + \frac{1}{2}O_2$). During charge, Mg^{2+} ions can be reduced to Mg atoms and also I^- ions oxidized to I_3^- in aprotic solvents. The I^-/I_3^- redox couple can catalyze charge/discharge processes of SMABs.

Inoishi et al. proposed a new concept of oxygen shuttle type batteries with solid oxide for MABs, which used a zirconium oxide that was stabled with calcium. They reported amount of open circuit potential and the discharge capacity was 1.18 V and 1154 mAh g^{-1} (about 50% of theoretical value), respectively [34]. Vardar et al. used magnesium aluminum chloride complex (MACC) for Mg/O_2 batteries. MACC simple salts from the reaction of magnesium with a Lewis acid in a nonaqueous solvent such as dimethoxy ethane (DME) or tetrahydro furan (THF) is prepared. They reported its high discharge capacity, but they compared to cells built with a Grignard/THF electrolyte, thus observed had more discharge capacity and lower recharge efficiency [35]. Khoo et al. used Trihexyl(tetradecyl) phosphonium chloride ionic liquid as an electrolyte in MABs and showed that the water content of ionic liquid plays a vital role in discharge characteristics [36]. In another study, Khoo et al. reported trihexyl(tetradecyl) phosphonium chloride ionic liquid as an electrolyte of MABs. The presented ionic liquid improves oxygen reduction current [37].

In this study, we mechanically prepared micro and nano scaled Mg powder in pure and composite form with carbon by using a home-made rotary ball mill. We compared the electrochemical performance of pure Mg and Mg/carbon composite with different particle sizes in both primary and secondary Mg/O_2 batteries.

2.EXPERIMENTAL

2.1. Materials
Commercially pure (>98.5 %wt) magnesium powder from Merck with 60-300 μm range of particles sizes (ROPS) and 180 μm mean particle size (MPS) was used for preparation of sub-micrometer and nanometer- sized Mg powder and Mg/carbon composites by ball milling method. The other chemicals were analytical grade and purchased from Merck, Fluka or Aldrich. Double distilled water was used in all experiments.

2.2. Instruments
A new rotary ball mill was developed by Karami research group in Payame Noor University. The tank of ball mill is a horizontal cylindrical with a 20 L volume (diameter 50 cm and length 10 cm). The tank and balls were made of stainless steel 316. The tank wad fixed and rotating of loading and, balls was performed by three symmetrical blades with angles of 120°. The rotation of the blades is done by an electric motor and the rotation speed is adjusted by a single-phase to three-phase inverter. Specification of the used balls in the invented ball mill is listed in Table 1.

Table 1. Diameter and number of used balls in ball mill.

Diameter (mm)	5	10	15	20	25	30
Number	120	60	30	20	10	5

In the designed ball mill, the crushing process of the samples was performed at the %67 of critical rotation speed (R_{crt}). The critical rotation speed of ball mill depends on diameter of tank. For the designed ball mill, the diameter of tank is 0.5 m. The critical rotation speed based on the following equation (Eq. 1) is calculated at 59.8 rpm. Therefore, the operation rotation speed is 40 rpm (%67 of 59.8 rpm).

$$R_{Crt} = \frac{42.3}{\sqrt{D}} \quad \text{(Eq. 1)}$$

All tests of the constructed batteries are performed by BTE06 automatic battery test unit (developed by Karami research group and also used in previous studies [38-40]). All cyclic voltammetry and impedance studies were done by Eco Chemie AutoLab PGSTAT12. Particle size distribution of the Mg and Mg/carbon composites was studied by the Malvern (ZS3600) dynamic light scattering (DLS) apparatus. Field emission scanning electron microscopy (FE-SEM) observations were utilized by using a TeScan–Mira III model made by the Czech Republic. In order to consider more carefully the shape and morphology of the sample nanoparticles, transmission electron microscope (TEM) imaging of the LEO model LEO912-AB was used.

2. 3. Procedure
2.3.1. Mg and Mg/carbon powders
Any pollutant in tank of ball mill was removed by crushing 500 g Mg powder for 3 h. The resulting magnesium powder was discarded and not used in any other experiment. At each load, 1000 g of micronized magnesium powder was filled into the ball mill, and after the purging of argon gas for 5 min, the loading valve and both inlet and outlet inert gas valves were closed. The ball mill was rotated for different periods to produce sub-micro powders up to nanopowder of Mg. To prevent from agglomerating of Mg and reaching to nanometer range, activated carbon with different ratios was added to Mg powder before ball milling. Scanning electron microscopy (SEM), transmission electron microscopy (TEM), dynamic light scattering (DLS) and X- ray diffraction (XRD) techniques were used to characterize Mg and Mg/carbon composites. All prepared Mg and Mg/carbon powders were used as anode materials of both PMABs and SMABs.

2.3.2. Battery container structure
In this study, a similar container structure was used for PMAB sand SMABs. Figure 1 shows the container structure of the designed batteries. In the presented structure, Optalloy (copper/zinc/tin alloy) was electroplated on brass current collector of anode [41-43]. The anode collector was fixed in the Teflon anode part. A hole exists on the anode collector to paste 1 g anode material. The carbon textile, coated with 0.5 mg cm^{-2} platinum on one side, was used as the cathode of batteries. Between the anode separator and the hydrophobic side of carbon textile, a space of 1 ml is designed to be filled with electrolyte. The scheme of designed battery container is shown in two assembled and disassembled form in Fig. 1.

2.3.3. Preparation of anode paste
The anode current collector (part g in Fig. 1) was fixed in the hole of the anode holder (part f in Fig. 1). After fixing the current collector in the hole of the anode holder, a hole with a diameter of 10 mm and a depth of 3 mm is left to fill the anodic active material paste. The anode paste formulation includes Mg powder (1.0 g), activated carbon powder (1 g) and polytetrafluoro ethylene (PTFE; 0.2 g) which is mixed with some battery electrolyte to obtain a homogeneous paste. In Mg/carbon composite anodes: Mg/carbon composite (1.2 to 2 g), activated carbon powder (0.8 to 0 g) and PTFE (0.2 g) is mixed with battery electrolyte. In all of anode pastes, weight of Mg is exactly 1 g and

weight of total carbon (carbon in composite and added activated carbon) is 1 g. The final paste is filled into the hole of anode. The prepared anodes are dried and cured at 70 °C under vacuum. A steel mesh (1 mm thickness and 100 mesh) was used as a cathode current collector. A carbon textile containing 0.5 mg cm^{-2} Pt on one side was utilized as a cathode electrode.

2. 3.4. Electrochemical measurements
2.3.4.1. Battery tests
In the designed batteries, aqueous solution includes 2 M magnesium chloride and 3 M sodium chloride and organic solution includes 0.2 M I$_2$ in DMSO were used as the battery electrolyte in PMABs and SMABs, respectively. After the batteries are assembled, the batteries were filled with proper electrolyte (PMABs with aqueous and SMABs with organic electrolytes) and allowed to rest for an hour so that the electrolyte penetrates the cured anode material. Then the volume loss of the electrolyte was compensated by adding amount of electrolyte. The first discharge of all the assembled PMABs was done with a constant current equal to %10 of the theoretical capacity of each battery (i$_{discharge}$= 0.1 C= 0.1×2200= 220 mA). The assembled SMABs were charge with current rate of 0.1 C and after 10 min rest, the batteries were discharged with current rate of 0.1 C.

In the cycle life studies, the charging and discharging of SMABs were performed with a current rate of 0.1C (i$_{charge}$= i$_{discharge}$= 0.1C). It should be mentioned that in the PMABs, for reusing of the battery, the fresh anode paste could be replaced with the discharged anode (it is called mechanically charge).

2.3.4.2. Electrochemical impedance studies
A three-electrode electrochemical cell with anode part of PMAB as working electrode, a Ag/AgCl reference electrode and platinum disk as counter electrode was assembled. Electrochemical impedance (EI) studies were used for both aqueous (different concentration of magnesium chloride and sodium chloride in distilled water) and nonaqueous (different concentration of I$_2$ in DMSO) solutions. To perform EI experiments, in aqueous and organic (nonaqueous) electrolytes, double junction vessel of reference electrode was filled with solutions of 0.2 M I$_2$ in DMSO and 2 M magnesium chloride and 3 M sodium chloride, respectively. EI experiments were done at OCP in the frequency range of 0.5 Hz to 100 kHz with 10 mV (rms) of perturbation amplitude.

2.3.4.3. X-Ray diffraction studies
X-ray diffraction (XRD) was used to identify the crystalline phases of anode materials before and after charge/discharge cycles of the batteries.
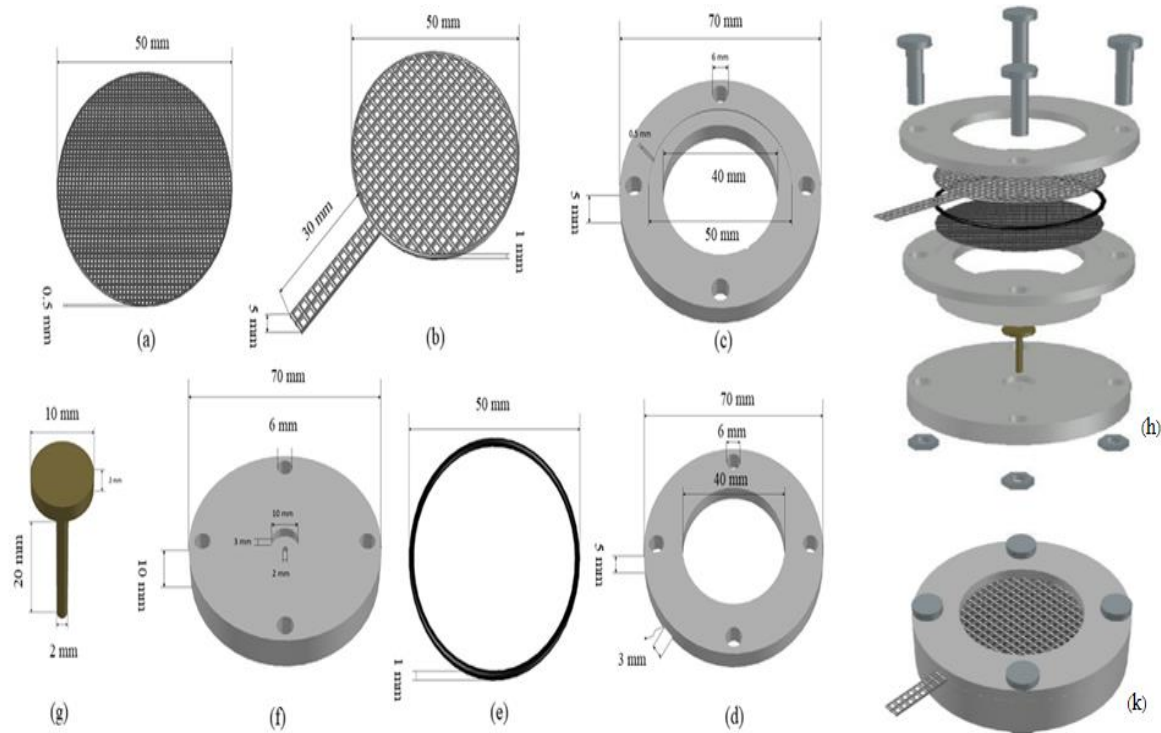
Fig. 1. Dimensions of parts of battery container: (a: Platinum coated carbon textile, b: Stainless steel mesh, c: Cathode holder, d: Electrolyte container, e: rubber O-ring, f: Anode holder and g: Anode current collector. The scheme of the disassembled battery container (h) and the assembled battery container (k).

3. RESULTS AND DISCUSSION

3.1. Mechanically prepared Mg and Mg/carbon composite powders

Eight Mg samples and eight Mg/carbon composite samples as anode materials of Mg-air batteries were prepared by the designed ball mill according to Table 2.

Each prepared sample was studied by DLS to determine the particle size distribution. Figures 2 show the DLS diagrams of the prepared Mg samples. As Fig 2 shows, in Mg samples (T_1, T_2, T_3, T_4, T_5, T_6, T_7, and T_8), by increasing milling time from 0 to 72 h, the MPS of Mg samples decreases from 180 to 0.17 µm but, by increasing the milling time from 72 to 96 h, the MPS increases from 0.17µm to 0.47 µm. On the other hand, by increasing milling time from 0 to 96 h, the ROPS decreases from 60-300 µm to 0.07-1 µm. The investigation of MPS and ROPS variations during ball milling process shows that the agglomeration of crushed particles is began from milling time of 60 h. The agglomeration of the crushed particles cases to form large particles and consequently, two peaks appears in DSL diagrams. The results prove that the ball milling method to prepare pure Mg particles is limited to the ROPS and MPS of 0.1-2 µm and 0.17 µm, respectively. In the sample T_6 with the smallest MPS, about 20% of the particles has been agglomerated and formed big particles with MPS of 0.8 µm. To obtain narrower ROPS and smaller MPS, adding of an additive to prevent from agglomeration is necessary. Therefore, activated carbon as a suitable conductive additive was added to Mg powder before ball milling. Some different Mg/carbon ratios were examined.

Table 2. Experimental conditions for preparation of Mg and Mg/carbon composite samples as anode materials of PMABs and SMABs.

Sample code	Mg (g)	Activated carbon (g)	Argon purge (s)	Milling time (h)
T_0	1000	0	0	0
T_1	1000	0	300	12
T_2	1000	0	300	24
T_3	1000	0	300	36
T_4	1000	0	300	48
T_5	1000	0	300	60
T_6	1000	0	300	72
T_7	1000	0	300	84
T_8	1000	0	300	96
T_9	500	500	300	36
T_{10}	500	500	300	48
T_{11}	500	500	300	60
T_{12}	500	500	300	72
T_{13}	500	500	300	96
T_{14}	600	400	300	72
T_{15}	700	300	300	72
T_{16}	800	200	300	72
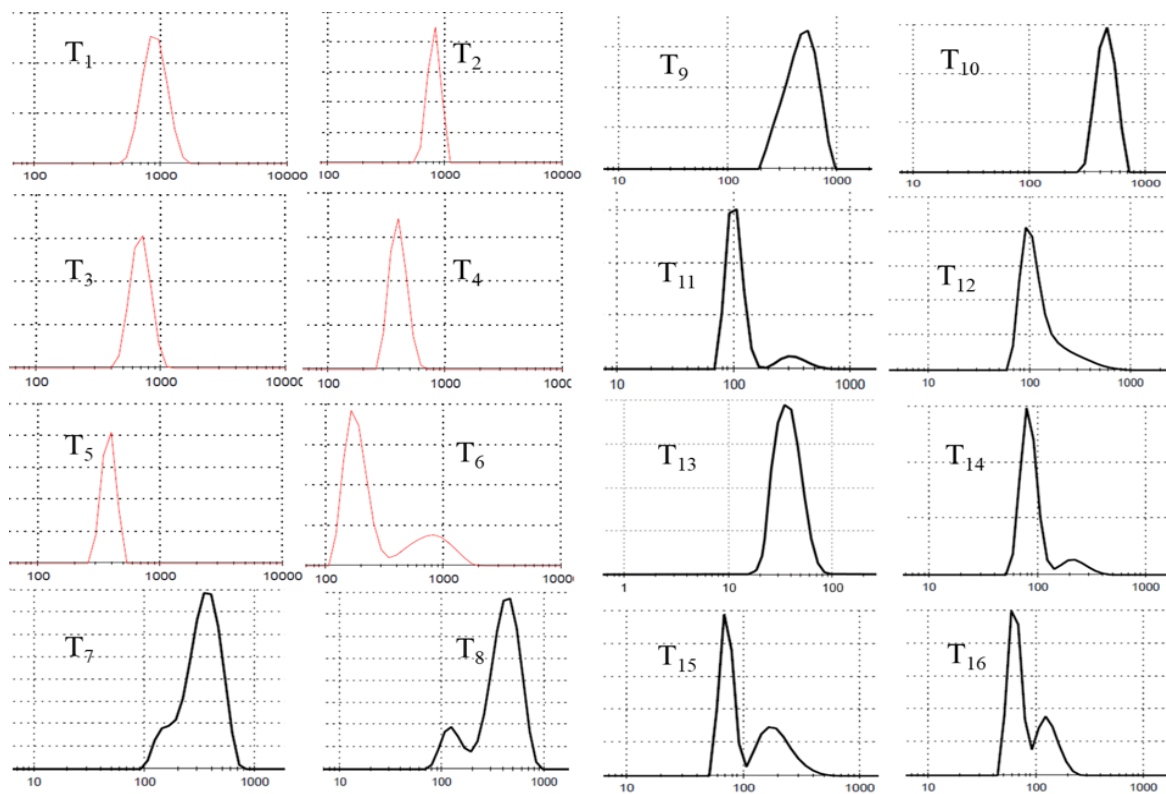
Fig. 2. DLS diagrams of Mg and Mg/carbon composite samples. In all the diagrams, the horizontal and vertical axes are in particle size (nm) and inNumber (%), respectively. Sample codes are according to Table 2.

To characterize the morphology of the Mg samples, the samples T_0, T_1, T_2, T_3, T_4, T_5, T_6, T_7, and T_8 (According to Table 2) were scanned by scanning electron microscope (SEM). To avoid displaying similar SEM images, only the SEM images of four samples (T_2, T_4, T_6 and T_8) were shown in Fig 3. As Fig. 3 shows, samples contain irregular and crushed particles, and the shape and morphology of the particles are almost the same in all four samples. By increasing the milling time from 24 hours to 96 hours, the diameter of the sample particles decreases from rage 5 to 20 μm in sample 2 to range 0.5 to 2 μm in sample 8. In addition to the above discussion, Fig 4 shows that agglomeration of the Mg particles is clearly seen in sample T_6 and especially in sample T_8. The SEM images confirm the presented DLS results.
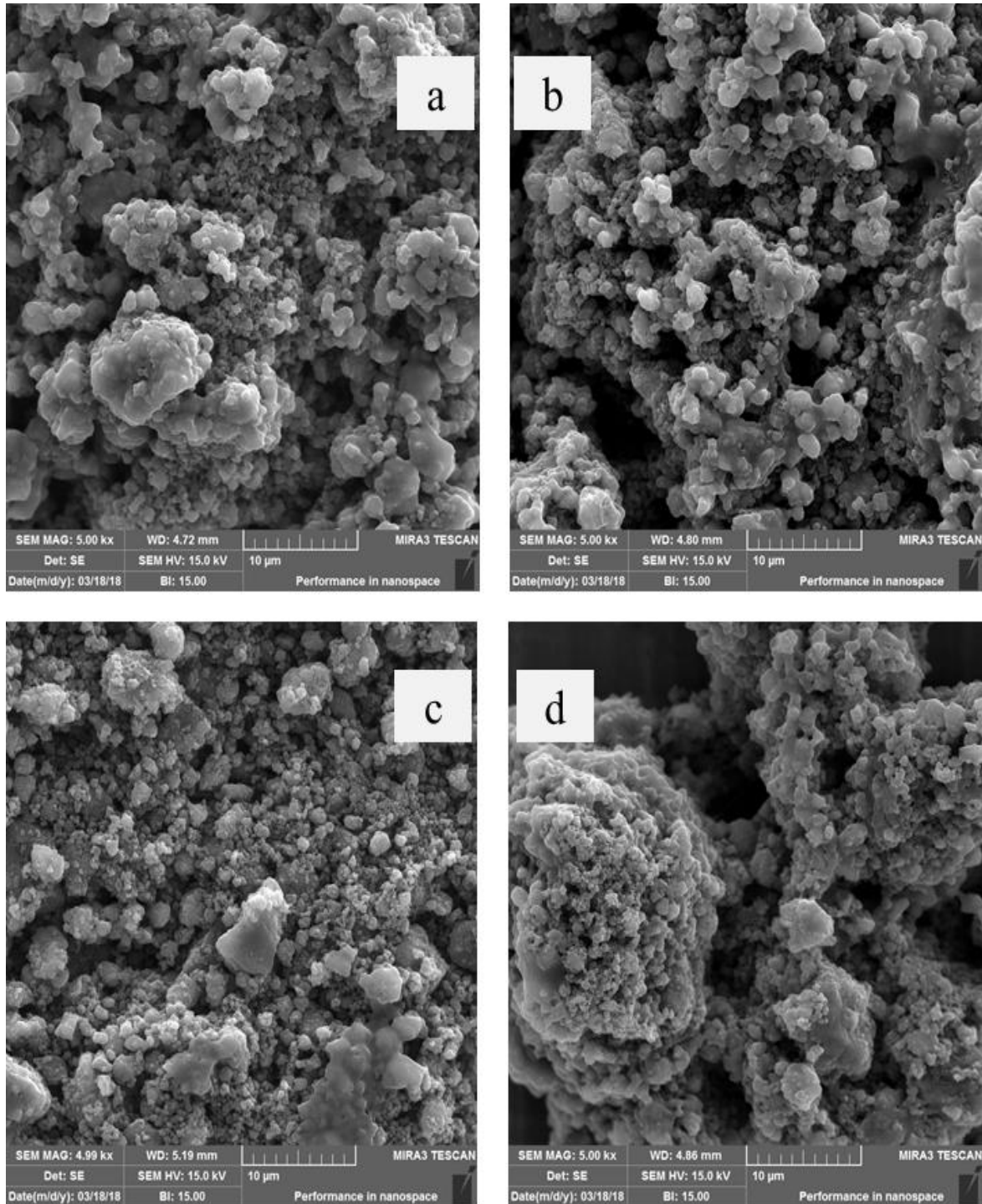
Fig. 3. SEM images of samples T_2, T_4, T_6 and T_8 according to Table 2.

The DLS diagrams of Mg/carbon composites (with different ratios of Mg/carbon and with different crushing times) were shown in Fig 2. In the experimental set, different ratios of Mg/carbon (0, 0.25, 0.43, 0.67, and 1) were examined at milling time of 72 h (samples: T_6, T_{16}, T_{15}, T_{14}, and T_{12}, respectively). The data of Figures 2 shows that at constant milling time of 72 h, The ROPS and MPS is decreased when, the Mg/carbon ratio is increased from 0 to 1. On the other hand, by increasing the amount of carbon, the agglomeration of smaller particles is decreased (the height and surface area under the second peak in DLS diagrams decreases). Therefore, the Mg/carbon ratio 1 is selected as optimum amount for further studies. At Mg/carbon ratio of 1, the samples T_9, T_{10}, T_{11}, T_{12} and T_{13} were crushed at different milling times of 36, 48, 60, 72 and 96 h, respectively. The DLS diagrams of these samples in Fig 2 confirmed that the milling time is main factor which can be used as controlling agent in preparation of Mg/carbon composites with different ROPS and MPS. Increasing time of milling causes to decrease the ROPS and MPS. For saving of time and energy, longer milling time than 96 h does not examined.

Table 3. Experimental conditions and DLS results of the prepared Mg and Mg/carbon composite samples as anode materials of PMABs and SMABs.

Sample code	ROPS (µm)	MPS (µm)
T_0	60-300	180
T_1	0.5-1.8	0.8
T_2	0.5-12	0.75
T_3	0.5-1.1	0.65
T_4	0.27-0.7	0.4
T_5	0.26-0.55	0.36
T_6	0.1-2	0.17
T_7	0.095-0.8	0.35
T_8	0.07-1	0.47
T_9	0.2-1	0.52
T_{10}	0.27-0.72	0.47
T_{11}	0.070-0.70	0.11
T_{12}	0.06-0.70	0.091
T_{13}	0.017-0.09	0.035
T_{14}	0.05-0.40	0.082
T_{15}	0.05-0.55	0.071
T_{16}	0.045-0.25	0.062

To evaluate the effect of carbon/Mg ratio on the particle size distribution, five samples (T_6, T_{16}, T_{15}, T_{14} and T_{12}) with different carbon/Mg ratios (0, 0.25, 0.43, 0.67 and 1, respectively) are prepared at same ball milling time. The DLS diagrams of these samples in Fig 2 show that the agglomeration of Mg particles increases with the decrease of the carbon/Mg ratio from 1 to 0. The obtained results confirm that the choice of activated carbon as an anti-agglomeration additive is correct. All results of DLS studies were summarized in Table 3. To obtain more information on the shape and size of the Mg/carbon composite samples, the samples were investigated with transmission electron microscopy (TEM) and the obtained electron micrographs were shown in Figure 4. The Mg/carbon ratio in five samples (T_9, T_{10}, T_{11}, T_{12} and T_{13}) is 1, but this ratio into samples of T_{14}, T_{15} and T_{16} is 0.67, 0.43 and 0.25, respectively. Based on TEM images, by increasing milling times from 36 to 96 h, the spherical shape particles of samples are only crushed to smaller spherical particles. By decreasing Mg/carbon ratio, agglomeration of particles increases (See TEM images of T_{14}, T_{15} and T_{16} in Fig 4).
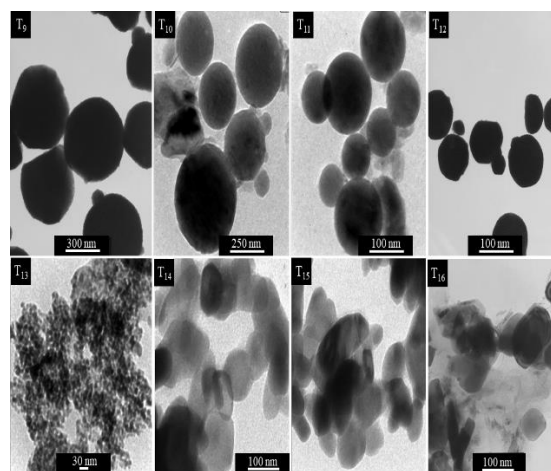
Fig. 4. TEM images of samples T_9, T_{10}, T_{11}, T_{12}, T_{13}, T_{14}, T_{15} and T_{16} according to Table 2.

3.2. Electrochemical studies

3.2.1. Application of the purchased Mg powder as anode material of both PMAB and SMAB

The first step of battery experiments, the commercial Mg powder (purchased from Merck) was mixed with activated carbon powder and PTFE and used as anode material of both PMAB and SMAB without any purification and any ball milling process. The assembled batteries were discharged at the current rate of 1C. The first discharge capacity of the PMAB and SMAB assembled with the commercial Mg powder to be 110 and 119.2 mA.h g^{-1}, respectively. Based on the obtained results, SMAB not only reveals higher discharge capacity than PMAB, but also has more mid- point voltage and can be recharged and reused. The obtained results can be seen in Fig. 5.

3.2.2. Application of the prepared Mg and Mg/carbon powders as anode materials of PMABs

In second step of battery experiments, all mechanically crushed Mg and Mg/carbon composite powders were applied as anode materials of PMABs as it described in the

experimental section (2.3.4.1). Each PMAB assembled with both Mg powder and Mg/carbon composite powder was discharged at a current rate of 1C. The discharge data of the Mg- based PMABs and Mg/carbon composite- based PMABs were shown in Fig. 5. As Fig. 5A shows, among prepared Mg anode materials, anode T_6 reveals higher discharge capacity because it includes the smallest Mg particles. It has been shown in other scientific reports that the use of smaller particles of electroactive materials can lead to a higher discharge capacity in different batteries [44,45]. The more agglomeration of Mg particles in

samples T_7 and T_8 causes to decrease their discharge capacities concerning to sample T_6. Figure 5B Shows the discharge capacities of PMABs assembled with Mg/carbon composite anodes. As it can be seen in Fig. 5B, at constant carbon/Mg ratio of 1, the discharge capacities of Mg/carbon composite anodes (T_9, T_{10}, T_{11}, T_{12}, and T_{13}) are increased from 238.3 to 418.6 mA.h g^{-1} when the milling time is increased from 36 to 96 h. Based on the DLS results, discharge capacities are increased by decreasing both ROPS and MPS of Mg/carbon composites.
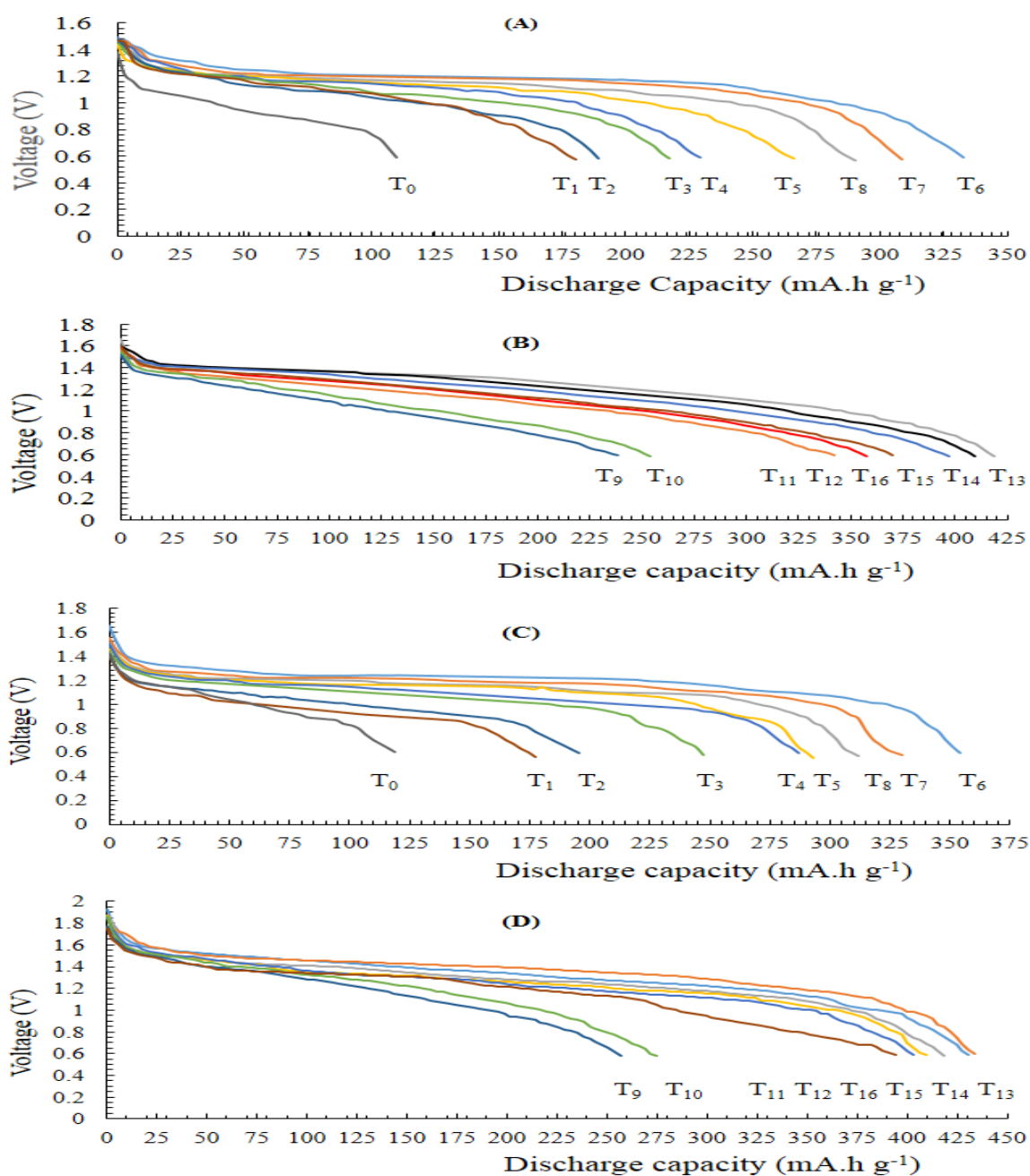
Fig. 5. Variation of battery voltage versus discharge capacity for the assembled PMABs and SMABs with Mg and Mg/carbon composite samples. A: Mg anodes in PMABs, B: Mg/carbon composite anodes in PMABs, C: Mg anodes in SMABs and D: Mg/carbon composite anodes in SMABs. All anode codes are according to Table 2.

3.2.3. Application of the prepared Mg and Mg/carbon powders as anode materials of SMABs

In 3rd step of battery experiments, to convert any type of magnesium oxide and hydroxide compound into metallic magnesium, each assembled SMAB was fully charged by current of 0.1 C for 2 h and then, the discharge data were recorded under current rate of 0.1 C. The discharge behaviors of SMBAs assembled with Mg powders and with Mg/carbon composite powders are shown in Figures 5C and 5D. As Fig 5C shows, discharge capacities of anode materials of T_1, T_2, T_3, T_4, T_5 and T_6 are different and are increased from T_1 to T_6 as well as particles sizes are decreased (See Figs 2 and 3). By increasing ball milling time from 72 h ($_{T6}$) to 84 h (T_7) and 96 h (T_8), the discharge capacities are decreased as well as particle sizes are increased. As Fig 5D shows, the discharge capacities of the SMABs assembled with anode materials of T_9, T_{10}, T_{11}, T_{12} and T_{13} are increased while the particles sizes of the samples are decreased (See Figs. 2 and 4 and Table 3). Based on data on Fig 5, open circuit voltage (OCV), min point voltage (MPV), discharge capacity (DC), power density (PD) and energy density (ED) were calculated and the results were summarized in Table 4.

3.2.4. Cycle life tests

In 4th step of the battery experiments, cycle life tests of the assembled SMABs were studied for 30 cycles. For all assembled SMABs, the discharge capacities were presented versus cycle numbers in Fig 6.

Table 4. Characteristics of the examined batteries.

Anode No.	OCV (V)		MPV (V)		DC (mA.h g^{-1})		PD (mW g^{-1})		ED (mW.h g^{-1})	
	PMAB	SMAB	PMAB	SMAB	PMAB	SMAB	PMAB	SMAB	PMAB	SMAB
T_0	1.383	1.421	0.922	1.005	110	119.167	2028.4	2211.0	101.42	119.763
T_1	1.466	1.401	1.082	0.947	180.278	177.22	2380.4	2083.4	195.061	167.827
T_2	1.477	1.421	1.073	1.007	189.444	195.556	2360.6	2215.4	203.273	196.925
T_3	1.482	1.432	1.039	1.076	216.944	247.500	2285.8	2367.2	216.944	266.310
T_4	1.492	1.503	1.017	1.091	229.167	287.222	2237.4	2400.2	233.063	313.359
T_5	1.441	1.461	0.976	1.15	265.833	293.333	2147.2	2530.0	259.453	337.333
T_6	1.475	1.651	0.714	1.221	333.056	354.444	157.8	2686.2	237.802	432.776
T_7	1.466	1.550	0.836	1.181	308.611	330.00	1839.2	2598.2	257.999	389.730
T_8	1.475	1.511	0.901	1.159	290.278	311.667	1982.2	2549.8	261.540	361.222
T_9	1.520	1.771	1.035	1.205	238.333	256.667	2277.0	2651.0	246.675	256.667
T_{10}	1.551	1.858	1.062	1.255	253.611	275.00	2336.4	2761.0	269.335	345.125
T_{11}	1.577	1.751	1.119	1.217	342.222	394.167	2461.8	2677.4	382.946	479.701
T_{12}	1.555	1.849	1.146	1.237	357.50	403.332	2521.2	2721.4	409.695	498.922
T_{13}	1.666	1.871	1.262	1.379	418.611	433.889	2776.4	3033.8	528.287	598.333
T_{14}	1.595	1.925	1.220	1.319	409.444	430.833	2684.0	2901.8	499.522	568.269
T_{15}	1.533	1.859	1.208	1.272	397.222	418.681	2657.6	2798.4	505.767	532.562
T_{16}	1.601	1.866	1.146	1.256	369.722	409.444	2521.2	2763.2	423.701	514.262
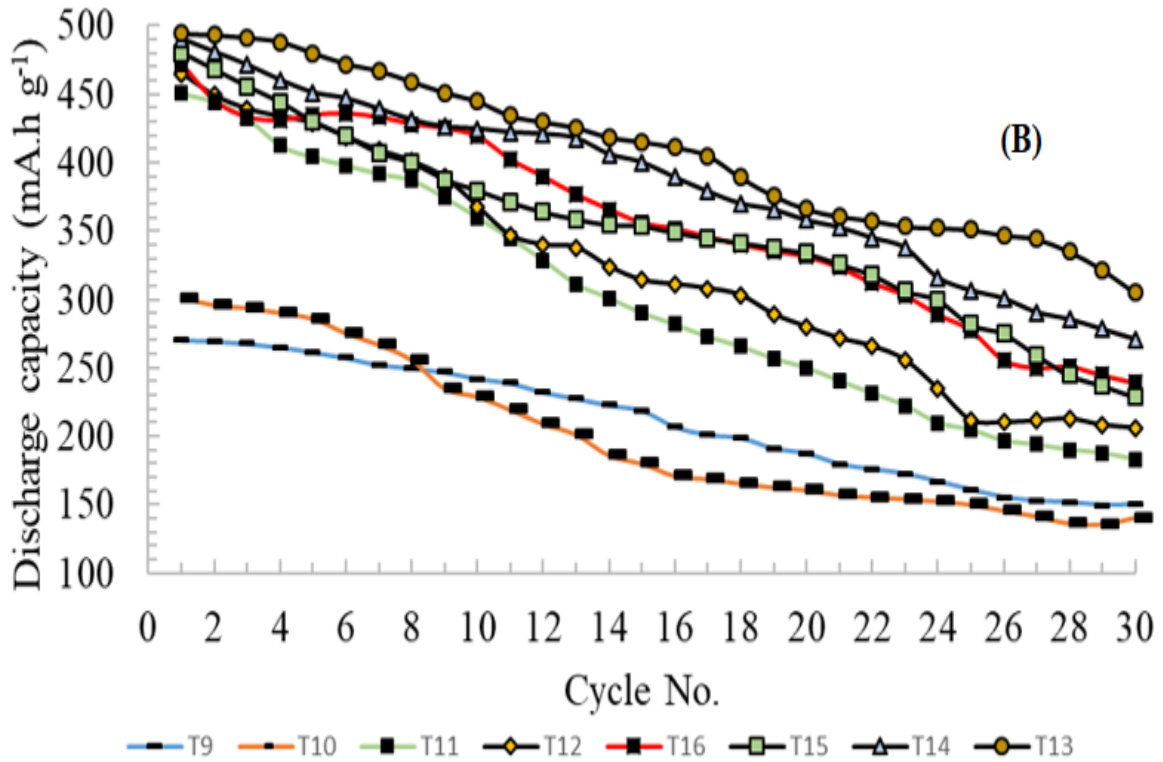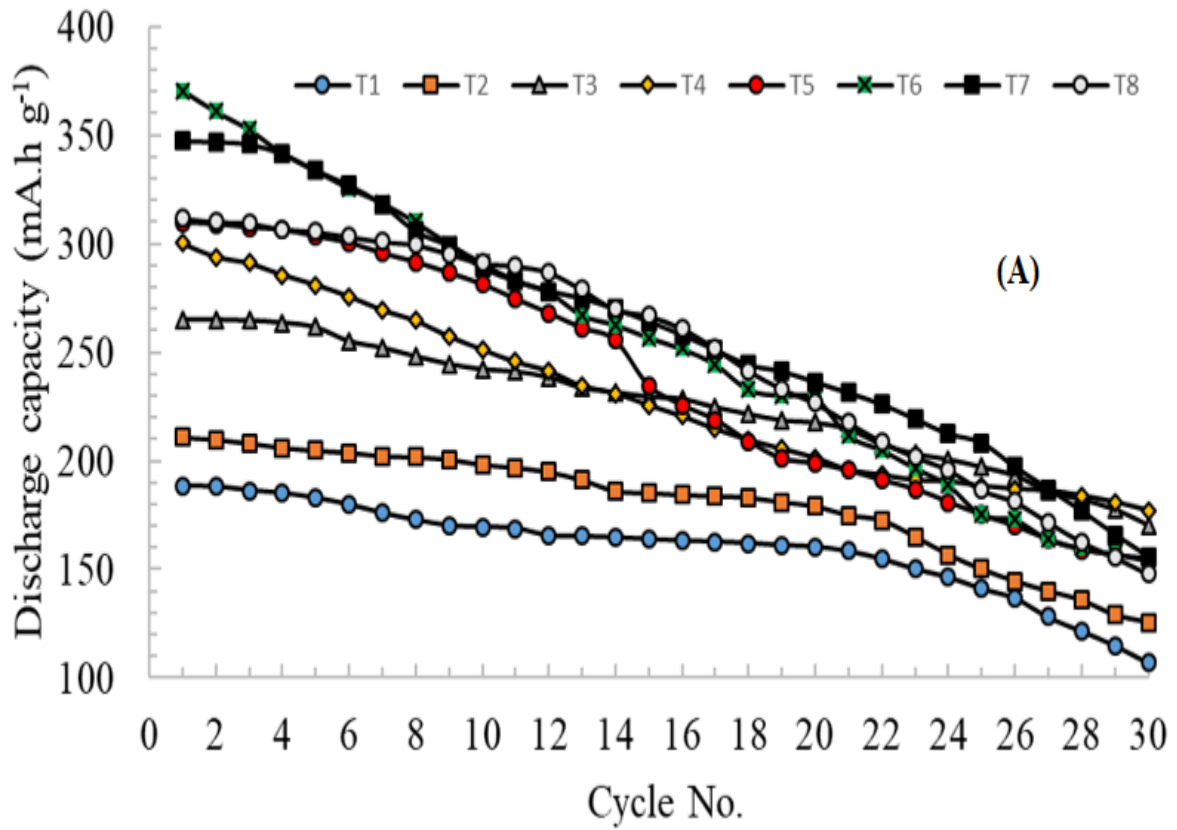
Fig. 6. Variation of discharge capacities versus charge/discharge cycle number for Mg samples (A) and Mg/carbon samples (B). All batteries were assembled with Mg powders according to Table 2.

There is a significant difference between the initial discharge capacities shown in Fig 5 and the first discharge capacities in life cycle tests where shown in Fig. 6. For example, based on Fig. 5C, the battery assembled with anode material of T_6 shows the discharge capacity of 354.44 mA.h g^{-1}, in comparison, discharge capacity of this battery in first cycle of Fig. 6 is 370.56 mA.h g^{-1}. For more clarification, the initial discharge capacities and the first discharge capacities in cycle life tests for all assembled rechargeable batteries are presented in Table 5.

Table 5. Discharge capacities in initial discharge and first cycle of cycle life tests for all assembled SMABs.

Anode code	Initial discharge capacity (mA.h g^{-1})	First discharge capacity in cycle life test (mA.h g^{-1})
T_1	177.22	188.123
T_2	195.556	210.667
T_3	247.500	265.45
T_4	287.222	300.11
T_5	293.333	309.789
T_6	354.444	370.56
T_7	330.00	347.11
T_8	311.667	311.77
T_9	256.667	270.541
T_{10}	275.00	301.14
T_{11}	394.167	450.491
T_{12}	403.332	465.01
T_{13}	433.889	494.087
T_{14}	430.833	490.125
T_{15}	418.681	480.134
T_{16}	409.444	471.71

These significant differences between initial discharge capacities and first discharge capacity in cycle life tests which presented in Table 5 are related to this fact that the discharged SMABs in Figs. 5C and 5D were reused for cycle life tests and were recharged at a current rate of 0.1 C. Therefore, the first capacity in the cycle life test is the second discharge of each battery. The first discharge capacities of the cycle life (Fig. 6) are larger than the initial discharge capacities of the batteries (Figs. 5C and 5D) are indicative of the fact that the initial charging of the batteries for 2 hours was not enough to charge fully the batteries and completely convert possible magnesium oxides and hydroxides on the surface of the anodes. Therefore, in the second charge for 10 hours (first cycle of cycle life test), the conversion of oxides and hydroxides into metallic magnesium is completed, and as a result, the battery is fully charged and the discharge capacity increases. To identify the effect of full charge on the anode composition, XRD patterns of anode material (T_{13}) were recorded in three charge states, including

discharge, initial partial charge and full charge (Fig 7). Figure 7 clearly shows that in discharge state, the anode mixture mainly includes MgO and $Mg(OH)_2$. In partial charge, besides metallic magnesium, a large amount of magnesium oxide and magnesium hydroxide is observed. When the battery is fully charged, the MgO and $Mg(OH)_2$ are converted to Mg.
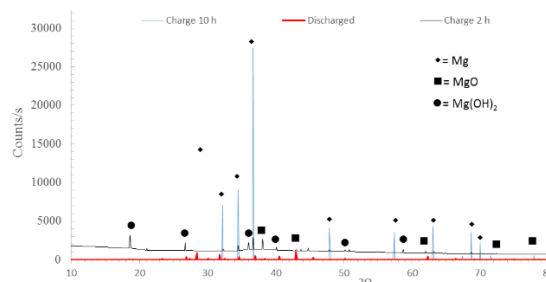
Fig. 7. XRD patterns of anode paste (T13) in three states including discharge, partial charge (2 h) and full charge (10 h).

3.2.4. Electrochemical impedance studies

Electrochemical Impedance Spectroscopy (EIS) studies of Mg-carbon composite as anode material (T_{13} in Table 2) in both aqueous and non aqueous electrolytes was carried out for evaluation of the Mg anode activity in the two different concentrations of electrolytes. All the EIS data were obtained at OCP. Thus, a direct correlation between the EIS data and the galvanostatically polarization condition during discharge process is not always feasible. Nevertheless, evolution of the EIS data with varying electrolyte concentration and also changing the electrolyte are benefit for understanding of the electrolyte type impact with anode interface on the dischargeabblity of Mg anode. EIS data were obtained in the frequencies range of 100 kHz to 0.5Hz. The instability is a consequence of the formation of significant volume of H_2 gas on Mg substrate with high activity that resulted in perturbation in anodic interface during the EIS data acquisation. The Nyquist plots at OCP after 1 h immersion in two concentrations of both aqueous and organic electrolytes are illustrated in Fig. 8. The respected Nyquist plots for both aqueous and organic electrolytes demonstrated two constant phase elements (CPE) with two time-constants at high and intermediate frequencies ranges. The first CPE at the high frequencies range is related to the formation of oxide/hydroxide film at the surface of Mg-carbon anode, whereas, the second CPE is attributed to the electron transfer reaction at the interface of the electrolyte and Mg-carbon anode [46,47]. Both CPEs have capacitive characteristics. Precarious condition is due to high corrosion rate and intense H_2 evolution (particular in aqueous

electrolyte) in close vicinity of the anode substrate lead to scattered points in Nyquist plots at low frequencies range. In aqueous electrolyte, some jumps can observed in spectra which is an artefact, because of H_2 bubbling during water reduction reaction. It should be mentioned that, such jumps are observable just when the whole measured impedance values are comparatively low. As frequencies approach to infinity, the electrolyte solution resistance (R_s) value obtained at Z_{real} axis. The R_s shift to the lower values with increasing salts and I_2 concentrations in aqueous and organic electrolytes, respectively. The total resistance (R_{total}) of the Mg-carbon anode surface can be evaluated by subtracting the $|Z|$ values at low and high frequencies as the characteristic parameter for analysis of Mg surface activity [48]. Thus, the lower R_{total} reveals the higher anode surface activity, which is a promising parameter for reaching an enhancement in voltage from the Mg-air battery and lower corrosion resistance [49,50] and also lower corrosion resistance [51].
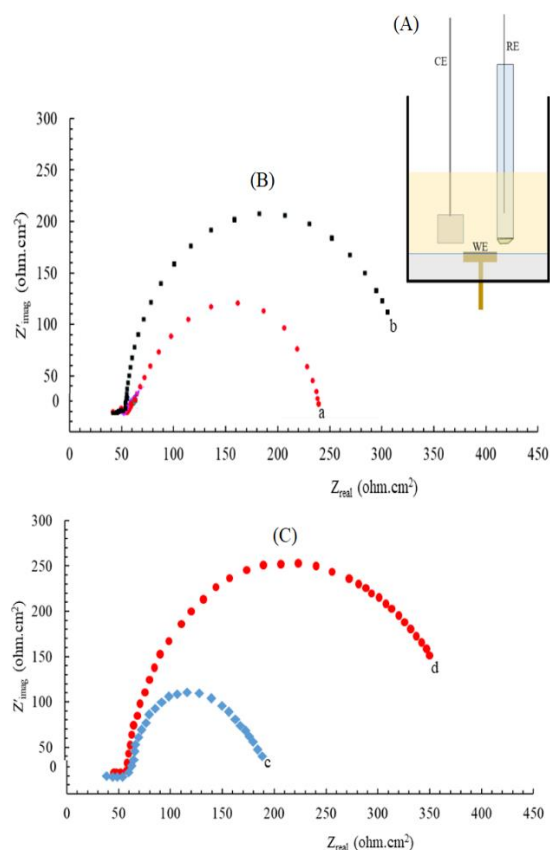
Fig. 8. Experimental cell for electrochemical impedance studies (A). In the scheme, CE, WE and RE are counter electrode, working electrode and reference electrode, respectively. Nyquist plot of Mg-carbon composite electrode (T_{13}) in aqueous (B) and organic (C) electrolytes. Nyquist plots of Mg-carbon composite electrode in 2 M $MgCl_2$ + 3 M NaCl (a), 1 M $MgCl_2$ + 1.5 M NaCl (b), 0.2 M I_2 in DMSO (c) and 0.1 M I_2 in DMSO (d).

4.CONCLUSION
The electrochemical performances of Mg and Mg-carbon composites as anode materials of primary and secondary Mg-air batteries were laborately investigated. Based on the obtained results, the following conclusions could be conducted:
1. The ball milling method can be used as laboratory and industrial method to prepare sub-micrometer and nanometer-sized Mg and Mg/carbon composite powders.
2. The particle size of anode material is an influential factor in the discharge capacity and cycle life of the Mg-air batteries.
2. The discharge capacity and cycle life of Mg-air batteries in I_2/DMSO organic electrolyte are better than those of aqueous electrolyte.
3. The Mg-air batteries in I_2/DMSO organic electrolyte are rechargeable.

REFERENCES
[1] A. Z. Alshaqsi, K. Sopian, and A. Al-Hinai, Review of energy storage services, applications, limitations, and benefits, *Energy Rep.* 6 (2020) 2886.

[2] Y. Li, J. Ma, G. Wang, Y. Zhu, Y. Song, and J. Zhang, Effect of Sodium Phosphate and Sodium Dodecyl benzene sulfonate on Discharge Performance of AZ31Magnesium Air Battery, *J. Chin. Soc. Corr. Prot.* 38 (2018) 587.

[3] Y. Li, X. Zhang, H. B. Li, H. D. Yoo, X. Chi, Q. An, J. Liu, M. Yu, W. Wang, and Y. Yao, Mixed-phase mullite electrocatalyst for pH-neutral oxygen reduction in MABs, *Nano Energy* 27 (2016) 8.

[4] L. J. Hardwick, and C. P. D. Leon, Rechargeable Multi-Valent Metal-Air Batteries, *Johnson Matthey Technol. Rev.* 62 (2018) 134.

[5] D. Ahuja, K. Varshney, and P.K. Varshney, Metal air battery: A sustainable and low cost material for energy storage, *J. Phys.* 1913 (2021) 012065.

[6] K. F. Blurton, and A. F. Sammells, Metal/air batteries: Their status and potential- a review, *J. Power Sources* 4 (1979) 263.

[7] D.A. Lowy, and B. Matyas, Sea Water Activated Magnesium-Air Reserve Batteries: Calculation of

Specific Energy and Energy Density for Various Cell Geometries, *J. Environ. Agri. Energ.* 1 (2020) 1.

[8] Tianran Zhang, Zhanliang Tao and Jun Chen, Magnesium–air batteries: from principle to Application, *Mater. Horiz.* 1 (2014) 196.

[9] R. Attias, and D. Aurbach, Anode- electrolyte interfaces in secondary magnesium batteries, *Joule* 3 (2019) 27.

[10] F. Tong, Sh.3 Wei, X. Chen, W. Ga0, Magnesium alloys as anodes for neutral aqueous MABs, *J. Magnes. Alloy* 9 (2021) 1861.

[11] L. Li, H. Chen, E. He, L. Wang, T. Ye, J. Lu, and Y. Jiao, J. Wang, R. Gao, H. Peng, Y. Zhang, High-Energy-Density MABs Based on Dual-Layer Gel Electrolyte, *Angew. Chem. Int. Ed.* 60 (2021) 15317.

[12] J. Ma, P. Hu, X. Jia, Ch. Zhang, and G. Wang, Organic/inorganic double solutions for magnesium–air batteries, *Royal Soc. Chem.* 11 (2021) 7502.

[13] T. Shiga, Y. Hase, Y. Kato, M. Inoue, K. Takechi, A rechargeable nonaqueous Mg–O2 battery, Chem. Commun. 52 (2013) 13753.

[14] Y. T. Lu, A. R. Neale, Ch. Hu, and L. J. Hardwick, Divalent Nonaqueous Metal-Air Batteries, *Front. Energ. Res.,* 8 (2021) 1-.

[15] N. Shrestha, K. Raja, V. Utgikar, Mg-RE Alloy Anode Materials for MABs Application, *J. Electrochem. Soc*. 16 (2019) 3139-.

[16] [16] D. Jia, F. Liu, D.Z. Yang, W. Wang, Research Progress of Magnesium Anode Materials and Their Applications in Chemical Power Sources, *Int. J. Electrochem. Sci*. 15 (2020) 10584.

[17] J. Ma, G. Wang, Y. Li, F. Ren, and A. A. Volinsky, Electrochemical performance of MABs based on AZ series magnesium alloys, *Ionics* 25 (2019) 2201.

[18] W. Li, Ch. Li, Ch. Zhou, H. Ma, J. Chen, Metallic Magnesium Nano/Mesoscale Structures: Their Shape-Controlled Preparation and Mg/Air Battery Applications, *Angew. Chem. Int. Ed*. 45 (2006) 6009.

[19] N. Wang, J. Liang, J. Liu, N. Q. Cai, J. Li, J. Chen, T. Huang, Z. Shi, CoFe nanoparticles dispersed in Co/Fe-N-C support with meso- and macroporous structures as the high-performance catalyst boosting the oxygen reduction reaction for Al/MABs, *J. Power Sources* 512 (2022) 230707.

[20] T. Fradi, O. Noureddine, F. B. Taheur, M. Guergueb, S. Nasri, et al., New DMAP meso-arylporphyrin magnesium(II) complex. spectroscopic, cyclic voltammetry and X-ray molecular structure characterization. DFT, DOS and MEP calculations and antioxidant and antifungal activities, *J. Molec. Struc*. 1236 (2021) 130299.

[21] R. Attias, M. Salama, B. Hirsch, Y. Goffer, and D. Aurbach, Anode-Electrolyte Interfaces in Secondary Magnesium Batteries, *Joule* 16 (2019) 27.

[22] G. Xin, X. Wang, Ch. Wang, J. Zheng, and X. Li, Porous Mg thin films for Mg–air batteries, *Dalton Trans*. 42 (2013) 1287.

[23] N. Wang, Y. NuLi, Sh. Su, J. yang, and J. Wang, Effects of binders on the electrochemical performance of rechargeable magnesium batteries, *J. Power Sources* 341 (2017) 219.

[24] B. Peng, J. Liang, Z. Tao, and J. Chen, Magnesium nanostructures for energy storage and conversion, *J. mater. Chem.* 19 (2009) 2877.

[25] A. F. Alharbi, A. A. M. Abahussain, M. H. Nazir, and S. Z. J. Zaidi, A High-Energy-Density Magnesium-Air Battery with Nanostructured Polymeric Electrodes, *Polymers* 14 (2022) 3187.

[26] H. Xu, N. Zou, and Q. Li, Effect of Ball Milling Time on Microstructure and Hardness of Porous Magnesium/Carbon Nanofiber Composites, *J. Min. Met. Mater. Soc.* 69 (2017) 1236.

[27] L. Han, Y. Zhang, Y. Guo, Y. Wan, L. Fan, M. Zhou, and G. Quan, Electrochemical behaviors and discharge performance of Mg-Sn binary alloys as anodes for MABs, *Mater. Res. Express* 8 (2021) 126531.

[28] F. Tong, X. Chen, T. Teoh, Sh. Wei, G. I. N. Waterhouse, W. Gao, Mg–Sn Alloys as Anodes for MABs, *J. Electrochem. Soc.* 168 (2021) 110531.

[29] Ch. Wu, X. Meng, and W. Wang, High-Performance Mg–Al–Bi Alloy Anode for Seawater Batteries and Related Mechanisms, *Processes* 8 (2020) 1362.

[30] Y. Yang, X. Xionga, J. Chen a, X. Peng, D. Chen, and F. Pan, Research advances in magnesium and magnesium alloys worldwide in 2020, *J. Magnes. Alloys* 9 (2021) 705.

[31] D. Shihirova, L. Wang, S.V. Lamaka, Ch. Wang, M. Deng, B. Vaghefinazari, D. Hoche, and M. L. Zheludkevic, Synergistic Mixture of Electrolyte Additives: A Route to a High-Efficiency Mg–Air Battery, *J. Phys. Chem. Lett.* 11 (2020) 8790.

[32] J. Park, K. Jang, S. Seo, J. Park, W. Kwon, and D. Kim, The study on the electrolyte circulation effect on Mg-air battery, *E3S Web of Conferences* 233 (2021) 01043.

[33] T. Shiga, Y. Hase, Y. Kato, M. Inoue, and K. Takechi, A rechargeable nonaqueous Mg–O2 battery, *Chem. Comm*. 49 (2013) 9152.

[34] A. Inoishi, Y. W. Ju, Sh. Ida, and T. Ishihara, Mg–air oxygen shuttle batteries using a ZrO2-basedoxide ion-conducting electrolyte, *Chem. Commun.* 49 (2013) 4691.

[35] G. Vardar, G. J. Smith, T. Thompson, K. Inagaki, J. Naruse, H. Hiramatsu, A. E. S. Sleightholme, J. Sakamoto, D. J. Siegel, and Ch. W. Monroe, Mg/O2 Battery Based on the Magnesium−Aluminum ChlorideComplex (MACC) Electrolyte, *Chem. Mater.* 28 (2016) 7629.

[36] T. Khoo, P. C. Howlett, M. Tsagouria, and D. R. MacFarlane, M. Forsyth, The potential for ionic liquid electrolytes to stabilise the magnesium interface for magnesium/air batteries, *Electrochem. Acta* 58 (2011) 583.

[37] T. Khoo, A. Soomers, A. A. J. Thorriero, and D. R. MacFarlane, Discharge behaviour and interfacial properties of a magnesium battery incorporating trihexyl(tetradecyl) phosphonium based ionic liquid electrolytes, *Electrochem. Acta* 87 (2013) 701.

[38] H. Karami, and F. Taala, Synthesis, characterization and application of $Li_3Fe_2(PO_4)_3$ nanoparticles as cathode of lithium-ion rechargeable batteries, *J. Power Sources* 196 (2011) 6400.

[39] H. Karami, and A. Mohammadi, Poly Vinyl Alcohol- Based Sol- Gel Synthesis of V2O5 Nanoflakes as Positive Electrodes of Li- ion Batteries, *Int. J. Electrochem. Sci.* 10 (2015) 7392.

[40] H. Karami, and M. Ghamooshi- Ramandi, Pulse Galvanostatic Synthesis of Zinc-Sulfur Nanocomposites and Application as a Novel Anode Material of Rechargeable Zinc-Manganese Dioxide Alkaline Batteries, *Int. J. Electrochem. Sci.* 7 (2012) 2091.

[41] H. Karami, M. F. Mousavi, and M. Shamsipur, A novel dry bipolar rechargeable battery based on polyaniline, *J. Power Sources,* 124 (2003) 303.

[42] H. Karami, M. F. Mousavi, M. Shamsipur, and S. Riahi, New dry and wet Zn-polyaniline bipolar batteries and prediction of voltage and capacity by ANN, *J. Power Sources* 154 (2006) 298.

[43] H. Karami, M. F. Mousavi, M. Shamsipur, A new design for dry polyaniline rechargeable batteries, *J. Power Sources* 117 (2003) 255.

[44] H. Sh. Majdi, Z. Azgarovich Latipov, V. Borisov, N. O. Yuryevna, M. M. Kadhim, W. Suksatan, I. H. Khlewee, and E. Kianfar, Nano and Battery Anode: *A Review, Nanoscale Res. Lett.* 16 (2021) 177.

[45] J. Liang, K. Xiao, R. Fang, A. Rawal, A. Lennon, and D. W. Wang, High volumetric capacity nanoparticle electrodes enabled by nanofluidic fillers, *Energy Stor. Mater.* 43 (2021) 202.

[46] L.G. Bland, A. D. King, N. Birbilis, and J. R. Scully, Assessing the corrosion of commercially pure Magnesium and commercial AZ31B by electrochemical impedance, mass-loss, Hydrogen collection, and inductively coupled plasma optical emission spectrometry solution analysis, *Corrosion* 71 (2015) 128.

[47] J. Yang, C. Blawert, S. V. Lamaka, K. A. Yasakau, L. Wang, D. Laipple, M. Schieda, S. Di, and M. L. Zheludkevich, Corrosion inhibition of pure Mg containing a high level of iron impurity in pH neutral NaCl solution, *Corrosion Sci.* 142 (2018) 222.

[48] Y.W.X. Zhang, L. Han, L.B. Ren, L.L. Fan, Y.Y. Guo, M.Y. Zhou, G.F. Quan, Effect of yttrium and calcium additions on electrochemical behaviors and discharge performance of AZ80 anodes for Mg−air battery, *J. Power Sources* 32 (2015) 449.

[49] Y. Ma, N. Li, D. Li, M. Zhang, and X. Huang, Performance of Mg–14Li–1Al–0.1Ce as anode for Mg-air battery, *J. Power Sources* 196 (2011) 2346.

[50] G. Huang, Y. Zhao, Y. Wang, H. Zhang, and F. Pan, Performance of Mg–air battery based on AZ31 alloy sheet with twins, *Mater. Lett.* 113 (2013) 46.

[51] M. Curioni, F. Scenini, T. Monetta, and F. Bellucci, Correlation between electrochemical impedance measurements and corrosion rate of magnesium investigated by real-time hydrogen measurement and optical imaging, *Electrochim. Acta* 166 (2015) 372.

پودرهای زیر میکرو و نانومتری منزیم و کامپوزیت منزیم-کربن تولید شده به روش مکانیکی به عنوان مواد آندی باتری های اولیه و ثانویه منیزیم- هوا

حسن کرمی*، فروزنده طلا، رضا بحجت منش اردکانی، محمدعلی کریمی

۱- بخش شیمی، دانشگاه پیام نور، تهران، ایران
* E-mail: karami_h@yahoo.com

چکیده

در این کار، پودرهای زیر میکرومتر و نانومتری منزیم و کامپوزیت منزیم/کربن به عنوان آن باتری‌های منیزیم-هوا با استفاده از یک دستگاه آسیاب گلوله‌ای اختراعی تولید شده است. مطالعه نمونه‌های تولید شده به کمک دستگاه‌های پراکندگی نور دینامیکی، میکروسکوپ الکترون روبشی، میکروسکوپ الکترونی عبوری و پراش اشعه ایکس انجام شد. اثرات زمان آسیابکاری و مقدار افزودنی کربن بر اندازه ذرات نمونه‌ها و نیز بر ظرفیت‌های دشارژ و سایر شاخص‌های الکتروشیمیایی هر دو نوع باتری اولیه و ثانویه منیزیم-هوا ارزیابی شد. محلول آبی حاوی منیزیم کلرید ۲ مولار و سدیم کلرید ۳ مولار و محلول آلی حاوی ید مولکولی با غلظت ۰/۲ مولار در حلال دی‌متیل سولوکسید به ترتیب به عنوان الکترولیت‌های باتری‌های اولیه و ثانویه منیزیم-هوا استفاده شدند. نمونه منیزیم با کد T_6 با میانگین اندازه ذرات ۱۷۰ نانومتر و نمونه کامپوزیت منزیم/کربن با کد T13 با میانگین اندازه ذرات ۳۵ نانومتر بالاترین ظرفیت دشارژ را هم در باتری اولیه ($mA.h\ g^{-1}$ ۳۳۳/۱ و ۴۱۸/۶ $mA.h\ g^{-1}$) و هم در باتری ثانویه منزیم-هوا (۳۵۴/۴ $mA.h\ g^{-1}$ و ۴۳۳/۶۹ $mA.h\ g^{-1}$) نشان دادند. آزمون عمر چرخه‌ای بر روی تمام باتری‌های ثانویه منیزیم-هوا در طول ۳۰ چرخه انجام شد.

کلید واژه ها

باتری منیزیم-هوا؛ باتری قابل شارژ؛ نانوپودر منیزیم؛کامپوزیت منیزیم/کربن؛ آسیاب گلوله‌ای چرخشی.